Effect of Intraparticle Porosity and Double Layer Overlap on Electrokinetic Mobility in Multiparticle Systems

Guofang Chen and Ulrich Tallarek*

Institut für Verfahrenstechnik, Otto-von-Guericke-Universität Magdeburg, Universitätsplatz 2, D-39106 Magdeburg, Germany

Received August 18, 2003. In Final Form: October 11, 2003

We have performed a systematic experimental study of electrokinetic mobility depending on the mobile phase ionic strength (concentration of Tris buffer) using different, well-defined porous and, for reference behavior, nonporous silica-based spherical microparticles. Effects of both an intraparticle electrical double layer overlap and the porosity on electrophoretic mobility in dilute suspensions and electroosmotic mobility in fixed beds of the devised (non)porous particles were investigated. The electrokinetically consistent results demonstrate a substantially different behavior for the porous (i.e., permeable and conducting) particles with respect to nonporous (solid) spheres. It may be related to a porous particle's dipole coefficient via the intraparticle void volume and, strongly depending on mobile phase ionic strength, to the actual magnitude of electroosmotic flow jetted through a particle's interior. In contrast to the normal electrical double layer behavior observed for the solid spheres (continuous decrease of mobility with ionic strength), these competitive contributions give rise to pronounced maxima in the mobility of the porous spheres. Our results are in qualitative agreement with the theoretical analysis of Miller et al. [*J. Colloid Interface Sci.* **1992**, *153*, 237] which, depending on the double layer interaction within a porous aggregate of solid spheres, predicts (significantly) lower or higher mobilities with respect to an impermeable and nonconducting particle.

1. Introduction

When dielectric solid particles are contacted with electrolyte solution, an electrical double layer (EDL) develops at the solid−liquid interface, for example, due to ionizable groups of the material.[1,2] Associated with the EDL, electrokinetic phenomena in dense multiparticle systems based on the tangential motion of the liquid relative to the charged surface play an important role in many processes with a technological, environmental, or analytical relevance.[3−17] Potential applications include transport of bulk liquid through fixed particulate beds in microfluidics and capillary electrochromatography, as well as water removal from concentrated particle slurries and industrial and natural porous media by electroosmosis (EO) or the enhanced settling, that is, densification of agglomerates, particle separation, and removal of colloidal contaminants from aqueous suspensions by electrophoresis (EP). Following the application of an external electrical field, a liquid, locally charged in the fluid-side domain of the EDL, begins to move relative to the stationary surface of rigid multiparticle systems in the former case (EO), while the latter involves the motion of mobile charged particles with respect to a stationary liquid (EP).

Further stimulated by the increased number and potential of applications in the physical and life sciences, a generalized and refined description of electrokinetic phenomena, particularly EO and EP, either for isolated (usually spherical and hard) particles or in multiparticle systems, has received much attention over the past decades.[18−52] Addressed issues include the magnitude and distribution of surface charge and electrokinetic potential,

* To whom correspondence should be addressed. Fax: +49 (0)-391-67-12028. E-mail: ulrich.tallarek@vst.uni-magdeburg.de.

(1) Lyklema, J. *Fundamentals of Interface and Colloid Science. Vol. II*: *Solid−Liquid Interfaces*; Academic Press: London, 1995.
(2) Delgado, A. V.; Arroyo, F. J. In *Interfacial Electrokinetics and Electrophoresis*; Delgado, A. V., Ed.; Marcel Dekker: New York, 2002; Chapter 1.
(3) Marlow, B. J.; Rowell, R. L. *Langmuir* **1991**, *7*, 2970.
(4) Mosher, R. A.; Saville, D. A.; Thormann, W. *The Dynamics of Electrophoresis*; VCH: Weinheim, 1992.
(5) Probstein, R. F.; Hicks, R. E. *Science* **1993**, *260*, 498.
(6) Sauer, J. E.; Davis, E. J. *Environ. Sci. Technol.* **1994**, *28*, 737.
(7) Ho, S. V.; Sheridan, P. W.; Athmer, C. J.; Heitkamp, M. A.; Brackin, J. M.; Weber, D.; Brodsky, P. H. *Environ. Sci. Technol.* **1995**, *29*, 2528.
(8) Dittmann, M. M.; Wienand, K.; Bek, F.; Rozing, G. P. *LC−GC* **1995**, *13*, 800.
(9) Tsuda, T., Ed. *Electric Field Applications in Chromatography, Industrial and Chemical Processes*; VCH: Weinheim, 1995.
(10) Haber, S. *J. Colloid Interface Sci.* **1996**, *179*, 380.
(11) Acar, Y. B.; Ozsu, E. E.; Alshawabkeh, A. N.; Rabbi, M. F.; Gale, R. J. *CHEMTECH* **1996**, *26*, 40.
(12) Crego, A. L.; González, A.; Marina, M. L. *Crit. Rev. Anal. Chem.* **1996**, *26*, 261.
(13) Coletta, T. F.; Brunell, C. J.; Ryan, D. K.; Inyang, H. I. *J. Environ. Eng.* **1997**, *123*, 1227.
(14) Bruin, G. J. M. *Electrophoresis* **2000**, *21*, 3931.
(15) Colón, L. A.; Burgos, G.; Maloney, T. D.; Cintrón, J. M.; Rodríguez, R. L. *Electrophoresis* **2000**, *21*, 3965.
(16) Polson, N. A.; Hayes, M. A. *Anal. Chem.* **2001**, *73*, 312A.
(17) Radko, S. P.; Chrambach, A. *Electrophoresis* **2002**, *23*, 1957.
(18) Dukhin, S. S.; Shilov, V. N. *Dielectric Phenomena and the Double Layer in Disperse Systems and Polyelectrolytes*; Wiley: New York, 1974.
(19) Levine, S.; Neale, G. H. *J. Colloid Interface Sci.* **1974**, *47*, 520.
(20) Levine, S.; Neale, G.; Epstein, N. *J. Colloid Interface Sci.* **1976**, *57*, 424.
(21) O'Brien, R. W.; White, L. R. *J. Chem. Soc., Faraday Trans. 2* **1978**, *74*, 1607.
(22) O'Brien, R. W. *J. Colloid Interface Sci.* **1983**, *92*, 204.
(23) Van der Put, A. G.; Bijsterbosch, B. H. *J. Colloid Interface Sci.* **1983**, *92*, 499.
(24) Ohshima, H.; Healy, T. W.; White, L. R. *J. Chem. Soc., Faraday Trans. 2* **1983**, *79*, 1613.
(25) O'Brien, R. W.; Perrins, W. T. *J. Colloid Interface Sci.* **1984**, *99*, 20.
(26) Anderson, J. L. *J. Colloid Interface Sci.* **1985**, *105*, 45.
(27) Zukoski, C. F.; Saville, D. A. *J. Colloid Interface Sci.* **1986**, *114*, 32.
(28) Zukoski, C. F.; Saville, D. A. *J. Colloid Interface Sci.* **1986**, *114*, 45.
(29) O'Brien, R. W. *J. Colloid Interface Sci.* **1986**, *110*, 477.
(30) Kozak, M. W.; Davis, E. J. *J. Colloid Interface Sci.* **1986**, *112*, 403.
(31) O'Brien, R. W.; Ward, D. N. *J. Colloid Interface Sci.* **1988**, *121*, 402.
(32) Kozak, M. W.; Davis, E. J. *J. Colloid Interface Sci.* **1989**, *127*, 497.
(33) Yoon, B. J. *J. Colloid Interface Sci.* **1991**, *142*, 575.

10.1021/la0355141 CCC: $25.00
Published on Web 11/20/2003

the ratio of the particle diameter to the EDL thickness, particle polydispersity, EDL polarization and surface conductivity, particle volume fraction or, vice versa, the interparticle porosity, spatial distribution of particles (periodic arrays vs random structures), Stern layer dynamics, particle−particle interaction and an EDL overlap, adsorption effects, as well as properties of the electrolyte solution like mobility, valency, and concentration of ionic species. Assumptions inherent to the popular hard-sphere models are that the particles are essentially impermeable (nonporous) and nonconducting. This often seems appropriate inasmuch as conducting particles become polarized by the applied electrical field, preventing the passage of current through the particle and causing it to behave like a nonconductor. On the other hand, to realize a significantly increased surface-to-volume ratio almost exclusively porous particles are used in the analytical and engineering sciences where packed beds are encountered as solid phase support for the devised reaction, separation, or purification of target compounds in view of high sample throughput or its complexity and where, consequently, a larger specific surface area is usually required (between 100 and 1000 $m^2 g^{-1}$, depending on application and needed pore sizes).

Apart from applications such as ion exchange and preparative liquid chromatography in which the particles' spatio-temporal surface charge pattern and EDL characteristics also become important for the retention of charged (bio)molecules,[53−57] a relatively young separation technique still more closely related to the above-mentioned electrokinetic phenomena (EO and EP) is capillary electrochromatography (CEC).[58−65] It combines the separation of molecules based on their differential partitioning between a stationary and mobile phase with the electrokinetically driven transport of liquid (EO) and an additional selectivity offered by a differential migration of charged molecules in an electrical field (EP). Typically, the 75−150 μm i.d. fused-silica capillaries are packed with 3−10 μm spherical, porous particles and fields up to 10^5 V/m are applied for moving electrolyte solution and solute through the fixed bed. Most common stationary phases in CEC are porous silica supports with chemically bonded surface groups[66−68] where the amount and accessibility of residual silanols influence the surface charge density and extent of electroosmotic flow (EOF). Compared to conventional hydraulic flow, the EOF is basically used for far superior hydrodynamic dispersion characteristics which allow more efficient separation of complex samples. A substantial fraction of the total EOF proceeds through the particles, depending on the intraparticle EDL overlap,[69−75] and further, the electrical conductivity of a column can be used to evaluate intraparticle ion transport and permeability.[76] Thus, in addition to the void space between particles, the intraparticle pore space and its relevant morphological parameters such as porosity, the shape, size distribution, and connectivity of pores play an important role in the total transport of ions and bulk liquid through a bed of porous particles. Vice versa, when an originally solid particle becomes permeable and conducting, consequences result for its electrophoretic mobility. As predicted by Miller et al.[77] and later verified to some extent experimentally by Miller and Berg,[78] the electrophoretic mobility of porous particles is expected to differ substantially from that of identical nonporous particles (being impermeable and nonconducting).

Due to the importance of porous support media with a hierarchy of length scales and resulting EDL overlap in many applications involving electrokinetic phenomena and the circumstance that the hard-sphere assumptions are violated, as well as the fact that only a very few electrokinetic data are available for porous particles, we conducted a systematic experimental study of electrophoretic and electroosmotic mobilities by using (otherwise similar) nonporous and porous silica-based, spherical particles with a different intraparticle porosity and mean pore size. This allowed us to realize a wide range of experimental conditions under which the EDL appeared either thin or thick with respect to intraparticle pore dimensions. Results obtained for the particles' electrophoretic mobility are discussed in view of the theoretical

(34) Solomentsev, Y. E.; Pawar, Y.; Anderson, J. L. *J. Colloid Interface Sci.* **1993**, *158*, 1.
(35) Dukhin, A. S.; Van de Ven, T. G. M. *J. Colloid Interface Sci.* **1994**, *165*, 9.
(36) Kang, S.-Y.; Sangani, A. S. *J. Colloid Interface Sci.* **1994**, *165*, 195.
(37) Ohshima, H. *J. Colloid Interface Sci.* **1997**, *188*, 481.
(38) Liu, Y. C.; Keh, H. J. *Langmuir* **1998**, *14*, 1560.
(39) Ennis, J.; Anderson, J. L. *J. Colloid Interface Sci.* **1997**, *185*, 497.
(40) Lee, E.; Chu, J.-W.; Hsu, J.-P. *J. Colloid Interface Sci.* **1999**, *209*, 240.
(41) Dukhin, A. S.; Shilov, V.; Borkovskaya, Y. *Langmuir* **1999**, *15*, 3452.
(42) Johnson, T. J.; Davis, E. J. *J. Colloid Interface Sci.* **1999**, *215*, 397.
(43) Ohshima, H. *J. Colloid Interface Sci.* **1999**, *210*, 397.
(44) Shugai, A. A.; Carnie, S. L. *J. Colloid Interface Sci.* **1999**, *213*, 298.
(45) Lee, E.; Lee, Y.-S.; Yen, F.-Y.; Hsu, J.-P. *J. Colloid Interface Sci.* **2000**, *223*, 223.
(46) Wei, Y. K.; Keh, H. J. *Langmuir* **2001**, *17*, 1437.
(47) Ding, J. M.; Keh, H. J. *J. Colloid Interface Sci.* **2001**, *236*, 180.
(48) Carrique, F.; Arroyo, F. J.; Delgado, A. V. *J. Colloid Interface Sci.* **2002**, *252*, 126.
(49) Chih, M.-H.; Lee, E.; Hsu, J.-P. *J. Colloid Interface Sci.* **2002**, *248*, 383.
(50) Keh, H. J.; Ding, J. M. *Langmuir* **2002**, *18*, 4572.
(51) Lin, W.-H.; Lee, E.; Hsu, J.-P. *J. Colloid Interface Sci.* **2002**, *248*, 398.
(52) Carrique, F.; Arroyo, F. J.; Jiménez, M. L.; Delgado, A. V. *J. Phys. Chem. B* **2003**, *107*, 3199.
(53) Liu, H.; Cantwell, F. F. *Anal. Chem.* **1991**, *63*, 993.
(54) Hågglund, I.; Ståhlberg, J. *J. Chromatogr., A* **1997**, *761*, 3.
(55) Okada, T. *Anal. Chem.* **1998**, *70*, 1692.
(56) Ståhlberg, J. *J. Chromatogr., A* **1999**, *855*, 3.
(57) Dziennik, S. R.; Belcher, E. B.; Barker, G. A.; DeBergalis, M. J.; Fernandez, S. E.; Lenhoff, A. M. *Proc. Natl. Acad. Sci. U.S.A.* **2003**, *100*, 420.
(58) Walhagen, K.; Unger, K. K.; Hearn, M. T. W. *J. Chromatogr., A* **2000**, *887*, 165.
(59) Pyell, U. *J. Chromatogr., A* **2000**, *892*, 257.
(60) Tang, Q. L.; Lee, M. L. *Trends Anal. Chem.* **2000**, *19*, 648.
(61) *Capillary Electrochromatography*; Deyl, Z., Svec, F., Eds.; Elsevier: Amsterdam, 2001.
(62) Bartle, K. D.; Myers, P. *J. Chromatogr., A* **2001**, *916*, 3.
(63) Rathore, A. S. *Electrophoresis* **2002**, *23*, 3827.
(64) Mistry, K.; Krull, I.; Grinberg, N. *J. Sep. Sci.* **2002**, *25*, 935.
(65) Rapp, E.; Tallarek, U. *J. Sep. Sci.* **2003**, *26*, 453.
(66) Robson, M. M.; Cikalo, M. G.; Myers, P.; Euerby, M. R.; Bartle, K. D. *J. Microcolumn Sep.* **1997**, *9*, 357.
(67) Fujimoto, C. *Trends Anal. Chem.* **1999**, *18*, 291.
(68) Matyska, M. T.; Pesek, J. J.; Boysen, I.; Hearn, M. T. W. *Electrophoresis* **2001**, *22*, 2620.
(69) Venema, E.; Kraak, J. C.; Poppe, H.; Tijssen, R. *J. Chromatogr., A* **1999**, *837*, 3.
(70) Vallano, P. T.; Remcho, V. T. *Anal. Chem.* **2000**, *72*, 4255.
(71) Stol, R.; Poppe, H.; Kok, W. Th. *Anal. Chem.* **2001**, *73*, 3332.
(72) Tallarek, U.; Rapp, E.; Seidel-Morgenstern, A.; Van As, H. *J. Phys. Chem. B* **2002**, *106*, 12709.
(73) Dearie, H. S.; Smith, N. W.; Moffat, F.; Wren, S. A. C.; Evans, K. P. *J. Chromatogr., A* **2002**, *945*, 231.
(74) Tallarek, U.; Pačes, M.; Rapp, E. *Electrophoresis* **2003**, in press. DOI 10.1002/elps.200305673.
(75) Tallarek, U.; Rapp, E.; Sann, H.; Reichl, U.; Seidel-Morgenstern, A. *Langmuir* **2003**, *19*, 4527.
(76) Vallano, P. T.; Remcho, V. T. *J. Phys. Chem. B* **2001**, *105*, 3223.
(77) Miller, N. P.; Berg, J. C.; O'Brien, R. W. *J. Colloid Interface Sci.* **1992**, *153*, 237.
(78) Miller, N. P.; Berg, J. C. *J. Colloid Interface Sci.* **1993**, *159*, 253.

work by Miller et al.,[77] and they are confirmed by electroosmotic mobility measurements in packed capillaries.

2. Theoretical Background

In their theoretical analysis of the electrophoretic mobility μ_{EP} of a permeable, conducting porous particle, Miller et al.[77] considered a model spherical porous aggregate of radius R_s consisting of numerous, much smaller discrete hard spheres of radius r_s. Fluid flow within the randomly packed matrix of dielectric spheres was modeled with the Kuwabara form[79] of the unit cell model which had been adapted by Levine and Neale[19] for EOF through a bed (or swarm) of spheres. Thus, characteristic pore dimensions inside an aggregate depend on the diameter of the impermeable and nonconducting primary particles (of uniform size and shape), as well as on the particle volume fraction φ within the aggregate. The main result of the analysis by Miller et al.[77] was to predict the dependence of μ_{EP} on zeta-potential (ζ):

$$\mu_{EP} = \left(1 + \frac{\varphi}{2}\right)\left(\frac{2\epsilon_0\epsilon_r\zeta}{3\eta} + \frac{\epsilon_0\epsilon_r\psi_a F_{EO}}{3\eta}\right) \qquad (1)$$

where ϵ_0, ϵ_r, and η are the permittivity of a vacuum and the relative permittivity and viscosity of the electrolyte solution, respectively. ζ is the shear plane potential exhibited by one of the discrete (and hard) primary particles when disconnected from the aggregate and subjected to an electrophoretic mobility measurement. ψ_a is the shear plane potential at the solid−liquid interface within a porous aggregate (which may be identified with ζ).[19]

Equation 1 results from a consideration of two phenomena.[77] First, the presence of conducting electrolyte in the aggregate introduces a normal component to the electrical field at its outer surface as field lines start bending toward the aggregate. This reduces the field's tangential component, but because the latter determines the aggregate's observable electrophoretic motion, μ_{EP} is expected to decrease compared to that of a solid particle. It becomes more pronounced as the amount of entrained conducting liquid increases. Second, the charged solid−liquid interface inside an aggregate enables the generation of internal EOF. The factor F_{EO} in eq 1 takes into account the electroosmotic mobility with respect to an aggregate frame of reference. This jetting effect tends to increase μ_{EP}. While the rather complex expression for F_{EO} derived by Levine and Neale[19] does not need to be repeated here, a dependence of F_{EO} on r_s/λ_D at different porosities is shown in Figure 1 because of its importance for the upcoming discussion in view of intraparticle EDL overlap. The EDL thickness is characterized via the Debye screening length (λ_D):[1,2]

$$\lambda_D = \left(\frac{\epsilon_0\epsilon_r RT}{F^2\sum_i z_i^2 c_{i,\infty}}\right)^{1/2} \qquad (2)$$

where R is the gas constant, T is absolute temperature, F is Faraday's constant, z_i is the valency of ionic species i, and $c_{i,\infty}$ is its concentration in electroneutral solution. Depending on the EDL overlap (represented by r_s/λ_D) and internal void space or porosity (with $\epsilon_{intra} = 1 - \varphi$), F_{EO}

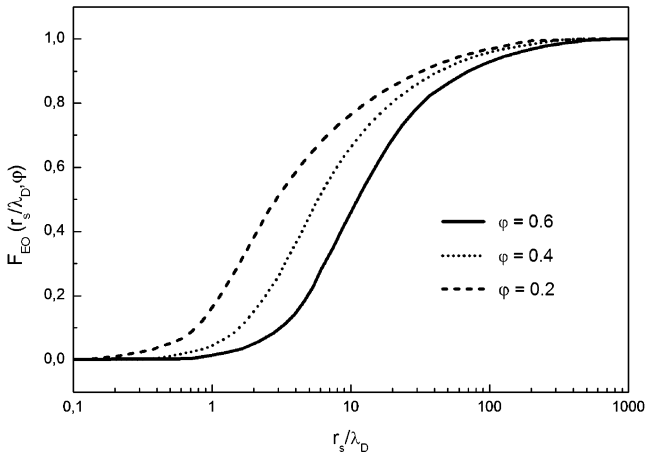

Figure 1. Electroosmotic flow factor F_{EO} vs r_s/λ_D for different void fractions $\epsilon_{intra} = 1 - \varphi$ in a spherical aggregate consisting of much smaller hard spheres with radius r_s and total solid volume fraction φ (adapted from Levine and Neale, ref 19).

gives the actual amount of EOF through an aggregate:[77]

$$\mathbf{u}_{EO} = -\frac{\epsilon_0\epsilon_r\psi_a\mathbf{E}}{\eta}F_{EO}(r_s/\lambda_D,\varphi) \qquad (3)$$

where $\mathbf{u}_{EO}$ and $\mathbf{E}$ are the volume-averaged fluid velocity and electrical field within the aggregate. Any pressure-driven flow through the porous aggregate is neglected. As demonstrated by Figure 1, F_{EO} for $0 < \varphi < 1$ asymptotically approaches zero and unity in the limits of $r_s/\lambda_D \to 0$ and $r_s/\lambda_D \to \infty$, respectively. While the lower limit corresponds to complete EDL overlap between neighboring unit cells of the model[77] or in the void space of a single porous particle, in general, the upper limit ($F_{EO} = 1$) is consistent with Smoluchowski's classical result for EOF within a porous medium of arbitrary pore geometry (when surface conductance is negligible) including porosity and pore size and shape.[80] Thus, $\mathbf{u}_{EO}$ decreases sharply as the EDL interaction in the porous aggregate increases. A similar behavior is recognized for EOF through open capillaries and the void space of random sphere packings.[81−85]

3. Experimental Section

Physical data of the (non)porous, spherical-shaped C18-silica particles relevant to the present study are summarized in Table 1. As can be seen, while these particles have an almost identical averaged diameter, the intraparticle porosity and mean pore sizes are systematically varied which allowed us to address the influence of an intraparticle EDL overlap (r_{pore}/λ_D) and solid volume fraction (φ or $\epsilon_{intra} = 1 - \varphi$) in our measurements of electrophoretic and electroosmotic mobility. Silica-based particles were received as research samples from Merck KGaA (Darmstadt, Germany), together with mercury intrusion and nitrogen adsorption data needed for determining intraparticle pore volume and surface area, respectively. As the mean pore diameter increases, the surface-to-volume ratio decreases significantly, and it is expectedly least for nonporous particles. The size distributions were characterized on a CILAS 1180 laser particle size analyzer (CILAS, Marcoussis, France) using dilute suspensions in 2-propanol. All particles used in our work show the same surface chemistry. Part of the activated silanol groups of the original native silica material are covalently bonded to C18-chains by reaction with suitable silanes. They are responsible

(79) Kuwabara, S. *J. Phys. Soc. Jpn.* **1959**, *14*, 527.

(80) Smoluchowski, M. *Z. Phys. Chem.* **1918**, *93*, 123.
(81) Rice, C. L.; Whitehead, R. *J. Phys. Chem.* **1965**, *69*, 4017.
(82) Knox, J. H.; Grant, I. H. *Chromatographia* **1991**, *32*, 317.
(83) Wan, Q.-H. *Anal. Chem.* **1997**, *69*, 361.
(84) Cikalo, M. G.; Bartle, K. D.; Myers, P. *J. Chromatogr., A* **1999**, *836*, 35.
(85) Arulanandam, S.; Li, D. Q. *Colloids Surf., A* **2000**, *161*, 89.

Table 1. Physical Data for the (Non)Porous Silica-Based Particles

particles	d_p [μm][a]	V_{pore} [mL/g]	d_{pore} [nm][b]	ϵ_{intra}[c]	r_{pore}/λ_D[d]	A_s [m^2/g][e]
porous spheres	2.45	0.88	41	0.66	0.6−12.8	64.7
	2.46	0.65	105	0.59	1.6−32.8	21.1
	2.42	0.34	232	0.43	3.6−72.5	7.5
nonporous	2.45					ca. 1[f]

[a] Refers to the external surface-averaged value ($d_p = 2R_s$). [b] Mean intraparticle pore diameter based on mercury porosimetry ($d_{pore} = 2r_{pore}$). [c] Intraparticle porosity calculated according to $\epsilon_{intra} = (1 + (1/\rho_{SiO}V_{pore}))^{-1}$, with ρ_{SiO} (density of the silica skeleton) taken as 2.24 g/mL. [d] For the range of buffer concentrations encountered in this work (1×10^{-4} to 4×10^{-2} M Tris). [e] Specific surface area based on the nitrogen adsorption data. [f] Finite, albeit small, because of the solid particles' external surface area.

for the hydrophobic nature of these surfaces, while residual silanol groups provide the surface charge. For modern particle and bonding technologies, it is possible to reproduce both the surface coverage of the bonded phase and residual silanol activity within 3%.[86]

Electrophoretic mobilities were measured at 298 K on a Zetasizer 3000 (Malvern Instruments Ltd., Worcestershire, U.K.) based on standard operation. The reported values for μ_{EP} (simply the ratio of particle velocity to the applied electrical field) represent an average of five independent runs. For the acquisition of electroosmotic mobilities, the ratio of the EOF velocity to the applied electrical field, stationary sphere packings (i.e., fixed beds) had to be prepared. For this purpose, 100 μm i.d., 360 μm o.d. fused-silica capillaries (Polymicro Technologies, Phoenix, AZ) were packed according to the slurry technique[86] using a WellChrom K-1900 pneumatic pump (Knauer GmbH, Berlin, Germany). Slurries were made from 10 mg of dry material and 100 μL of ethanol under gentle ultrasonication for 10 min. Glass-lined metal tubing (500 μm i.d.) was used as a reservoir into which the slurries were injected for the packing process. The pressure then was adjusted between 150 and 350 bar with respect to mean intraparticle pore sizes to avoid particle damage during further compaction of the beds toward random close sphere packings. Temporary outlet frits for the packing were provided by prepunched glass-fiber filters fixed in the zero-dead-volume unions (Upchurch Scientific, Oak Harbor, WA) to which all open-tubular capillaries were first connected. After having forced water as the pushing liquid for about 20 min at selected pressure through the packed capillaries, desired bed lengths of between 30 and 40 cm were reached. The permanent inlet and outlet frits were prepared by controlled particle sintering via heating with an arc fusion splicer FSM-05S (Fujikura, Tokyo, Japan) in its prefusion mode. Finally, the remainder of the particles was washed out and the union was removed.

The packed capillary columns were assembled in a HP^{3D}CE capillary electrophoresis instrument (Hewlett-Packard, Waldbronn, Germany) which allowed us to generate gradients in electrical potential from 0 to 30 kV between both ends of a capillary column. Measurements were made at a controlled temperature of 298 K. Electroosmotic mobilities μ_{EO} were calculated using the actual potential drop over a bed and residence time distributions of an unretained, uncharged flow field marker (which provides the mobile phase linear velocity) transported through the column by molecular diffusion and EOF. Thiourea was used for that purpose, and the standard photodiode array detector of the instrument was used to monitor its absorbance at 235 nm. Thiourea samples prepared in running mobile phase were injected electrokinetically (+5 kV for 3 s). An external helium pressure of 10 bar was exerted on both inlet and outlet mobile phase vials for minimizing bubble formation. EOF velocities were measured at typically 10 different field strengths, with μ_{EO} calculated as the slope of a linear dependence. Development of Joule heat was negligible in these experiments.

Tris(hydroxymethyl)aminomethane (Tris) buffer solutions in 80:20 acetonitrile/water (v/v) were used as the liquid electrolyte.

(86) Neue, U. D. *HPLC Columns*: *Theory, Technology, and Practice*; Wiley-VCH: New York, 1997.

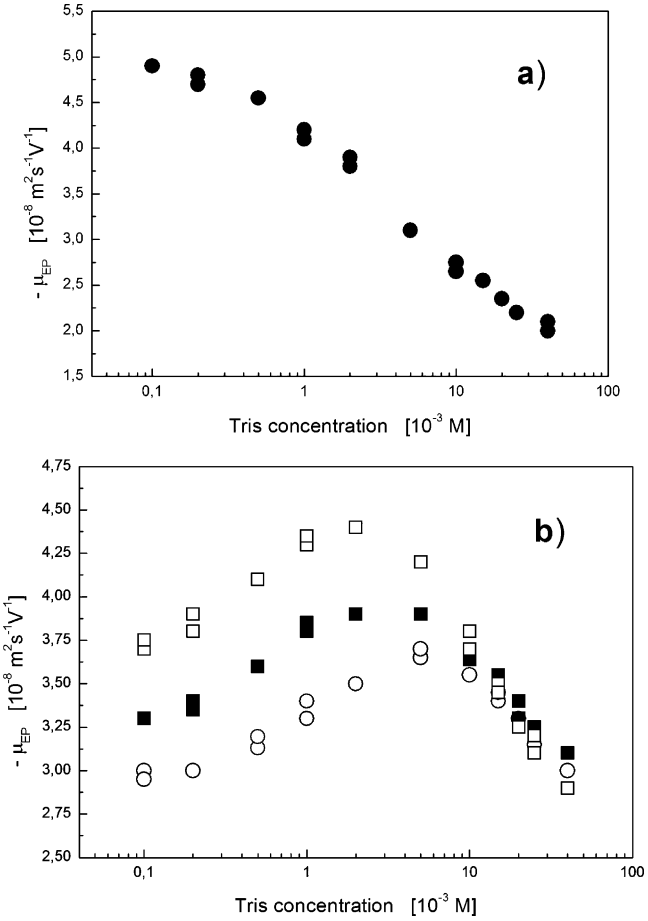

Figure 2. Electrophoretic mobility of the spherical-shaped, silica-based particles (Table 1) depending on the mobile phase concentration of Tris buffer: (a) nonporous particles (●); (b) porous particles with a mean intraparticle pore diameter (d_{pore}) of 41 nm (○), 105 nm (■), and 232 nm (□), respectively. The mobile phase ionic strength is half of the Tris concentration.

Mobile phases were filtered over a 0.45 μm nylon membrane filter and degassed by ultrasonication. An aqueous stock solution of 0.2 M Tris (the base form) was prepared using water purified on a Milli-Q-Gradient (Millipore GmbH, Eschborn, Germany), and the pH was adjusted to 8.3 by titration with concentrated hydrochloric acid. Appropriate volumes of this stock solution, MilliQ water, and HPLC grade acetonitrile were mixed to yield the Tris buffer solutions of desired ionic strength in 80:20 acetonitrile/water (v/v) covering the range from 1×10^{-4} to 4×10^{-2} M effective Tris concentration; for example, 2×10^{-3} M Tris in the final mobile phase corresponds to 0.01 M Tris in the aqueous part. The concentration of protonated Tris (acid form) needed for estimating the EDL thickness by means of λ_D (eq 2) was calculated from the Henderson−Hasselbalch equation with pH $\approx$ pK_a. For measurement of μ_{EO}, packed capillaries were preconditioned electrokinetically (using separate mobile phase vials) by applying a voltage of 5 kV for 10 min and then a voltage ramp up to 20 kV in 15 min and holding this final voltage over another 10 min. For measurement of μ_{EP}, 5 mg of the particles were suspended in 20 mL of degassed buffer under gentle ultrasonication, followed by overnight stirring in a rotary shaker. The relative permittivity (ϵ_r) and viscosity (η) at 298 K of the final 80:20 acetonitrile/water (v/v) electrolyte solutions were taken as 44.53 and 5.03×10^{-4} kg/(m·s), respectively.[87]

4. Results and Discussion

We first present results for electrophoretic mobilities and analyze individual contributions. Figure 2 demonstrates the influence of mobile phase Tris concentration

(87) Banholczer, A.; Pyell, U. *J. Chromatogr., A* **2000**, *869*, 363.

on μ_{EP} of the nonporous and porous silica-based particles (cf. Table 1 for particle characteristics). The dependence for nonporous spheres seen in Figure 2a reveals normal electrokinetic behavior in the sense that as the ionic strength of the liquid increases, the EDL is compressed, resulting in a reduced shear plane potential at the solid−liquid interface.[1] The thickness of the EDL remained small with respect to the particle radius over the whole range of buffer concentrations, that is, $38 < R_s/\lambda_D < 766$ (R_s denotes the radius of a macroscopic particle). Thus, the assumption of a thin EDL is valid on the particle scale ($R_s/\lambda_D \gg 1$) throughout the present study including all media. The continuously decreasing values of μ_{EP} at increasing Tris concentration (Figure 2a) then represent an electrokinetic behavior that is expected, at least qualitatively, for solid dielectric spheres with less significant contribution from surface conductance (over a range of mobile phase ionic strengths encountered in our work). It is noteworthy because conduction behind the shear plane may strongly influence and sometimes even overshadow usual EDL behavior, in particular at low electrolyte concentrations and higher values of ζ, leading to an increase of the electrokinetic mobility with ionic strength toward an intermediate, often just spurious maximum.[88−95] The magnitude of this effect further depends on the base material (although it has been predominantly investigated for polymer latices), surface modification, and post-treatments.

In striking contrast to the more or less familiar behavior of the hard spheres, the trend in μ_{EP} for the porous particles (Figure 2b) reveals distinct differences which obviously depend on the intraparticle porosity and actual extent of the EDL overlap and, thus, on the ratio r_{pore}/λ_D (the thin EDL assumption cannot be made inside these particles). With increasing concentration of Tris buffer from 1×10^{-4} M, the particle mobilities first increase and then move through a maximum at some particle-specific concentration between 1×10^{-3} and 1×10^{-2} M, followed by a decrease toward relatively common curves (above ca. 1×10^{-2} M Tris). Because all particles originated from the same base material, differences among porous spheres, as well as between the nonporous and porous spheres, in general, most probably can be related to the fact that porous particles are permeable for EOF and conducting depending on intraparticle porosity and pore sizes. To clarify the observed differences in view of these aspects, Figure 3 contrasts the typical behaviors. Here, the gray area separates regimes in which the mobility of either the nonporous or porous particles dominates over the other. At lower buffer concentrations, μ_{EP} for the solid spheres significantly exceeds that of any porous spheres encountered in this work (for clarity in a general comparison only the representative results for porous particles with $d_{pore} = 105$ nm are included in Figure 3). As indicated earlier, when an originally solid dielectric sphere is made permeable and conducting, the ratio of specific conductivities within the now-porous particle and bulk liquid

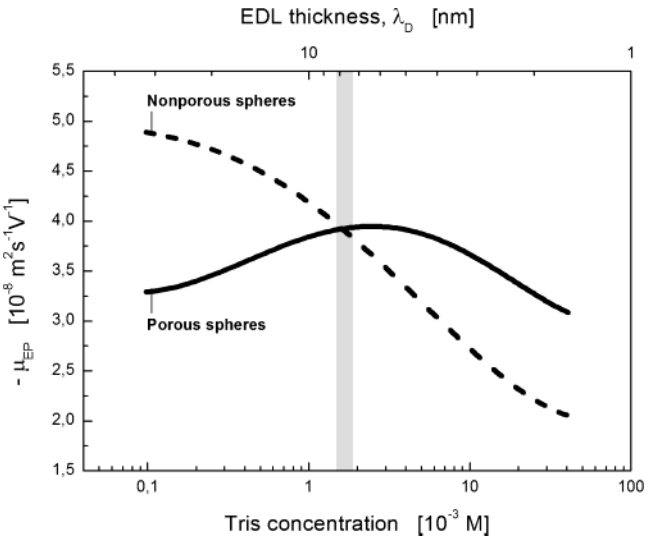

Figure 3. Comparison of spherical nonporous and porous ($d_{pore} = 105$ nm) silica-based particles in view of the electrophoretic mobilities depending on mobile phase ionic strength (which corresponds to half of the actual Tris concentration).

will increase from zero, bending electrical field lines toward the particle interior which reduces the tangential field component at a particle's external surface. Consequently, this contribution from the porosity effect reduces electrophoretic slip velocities associated with shear stress concentrated in the relatively thin EDL at the external solid−liquid interface, and it can explain the decreased values of μ_{EP} with respect to nonporous, dielectric spheres at lower buffer concentrations (Figure 3, between 1×10^{-4} and about 2×10^{-3} M Tris) where strong intraparticle EDL overlap prevails.

However, this contribution to μ_{EP} of the porous particles is more than compensated at increasing buffer concentration by the jetting effect due to intraparticle-forced EOF (relative to the solid skeleton of a particle and opposite to its electrophoretic motion). In contrast to the first effect, this phenomenon strongly depends on the buffer concentration and will begin to dominate μ_{EP} only when intraparticle EDL overlap is substantially reduced, enabling a significant amount of volumetric EOF through the particles (cf. F_{EO} in eq 1 and its dependence on r_s/λ_D in Figure 1). As evidenced by Figure 3, the jetting effect is responsible for an increasing mobility of permeable spheres between 1×10^{-4} and 2×10^{-3} M Tris (with $1.6 < r_{pore}/\lambda_D < 7.3$). The maximum in μ_{EP} then is a consequence of competitive contributions from this intraparticle EOF (increasing jetting effect) and the normal EDL behavior at the particles' external surface. The latter effect which ultimately dominates (leading to the decrease of μ_{EP} above 2×10^{-3} M Tris although EDL overlap continues to be further reduced) has already been recognized as the origin of a continuous mobility decrease at increasing buffer concentration for the nonporous spheres (Figure 2a). The presence of the jetting effect nevertheless can explain the finally higher values of μ_{EP} for these porous particles compared to the nonporous ones (see Figure 3 between 2×10^{-3} and 4×10^{-2} M Tris, with $7.3 < r_{pore}/\lambda_D < 32.8$).

To summarize, the unique dependence of electrophoretic mobilities of porous particles used in this work on ionic strength (Figure 2b) is a consequence of basically three contributions: (i) usual EDL behavior at the external particle surface leading to a decrease of mobility at increasing ionic strength, (ii) generation of intraparticle volumetric EOF (the jetting effect increases mobility at increasing ionic strength), and (iii) the dipole coefficient

(88) Van der Put, A. G.; Bijsterbosch, B. H. *J. Colloid Interface Sci.* **1983**, *92*, 499.
(89) Hidalgo-Álvarez, R.; Martín, A.; Fernández, A.; Bastos, D.; Martínez, F.; de las Nieves, F. J. *Adv. Colloid Interface Sci.* **1996**, *67*, 1.
(90) Lyklema, J.; Minor, M. *Colloids Surf., A* **1998**, *140*, 33.
(91) Folkersma, R.; van Diemen, A. J. G.; Stein, H. N. *Langmuir* **1998**, *14*, 5973.
(92) Johnson, P. R. *J. Colloid Interface Sci.* **1999**, *209*, 264.
(93) Löbbus, M.; van Leeuwen, H. P.; Lyklema, J. *Colloids Surf., A* **2000**, *161*, 103.
(94) Moncho, A.; Martínez-Lopez, F.; Hidalgo-Álvarez, R. *Colloids Surf., A* **2001**, *192*, 215.
(95) Hunter, R. *Adv. Colloid Interface Sci.* **2003**, *100*, 153.

of a porous particle which depends on its porosity but not on ionic strength. While the first contribution dominates overall mobility at higher ionic strengths (above 1×10^{-2} M Tris in Figure 2b) where, independent of actual intraparticle EDL overlap, mobilities for all porous particles are very similar and decreasing, the jetting effect, together with a different mean intraparticle pore size, is responsible for the increasing mobilities at lower ionic strengths and the different position of the maximum for μ_{EP} which shifts to higher ionic strength as the mean intraparticle pore size (and r_{pore}/λ_D) becomes smaller.

Based on the data in Figure 2b and Table 1, the actual porosity difference between particles, thereby referring to the last of the above-mentioned contributions, could also contribute to a shift of μ_{EP} to higher values at the increasing pore size because ϵ_{intra} concomitantly decreases. This would agree qualitatively with the theoretical analysis of Miller et al.[77] (eq 1), although the porosity, in addition, influences μ_{EP} oppositely via the jetting effect (Figure 1). In an intermediate regime of EDL interaction, both effects of a porosity difference (on the dipole coefficients and intraparticle EOF) may compensate each other or nearly so, while for sufficiently small and large values of r_{pore}/λ_D the former (conductivity) effect is expected to dominate.[77]

Before discussing these experimental results that have been obtained for the different particle porosities and systematic variation of intraparticle EDL overlap further in view of the work of Miller et al.,[77] we compare the dependence of μ_{EP} on ionic strength with the corresponding result for μ_{EO} summarized in Figure 4. These data confirm the substantially different electrokinetic behavior of porous versus nonporous spherical particles consisting of the same base material which has already been observed for μ_{EP} (Figure 2). In particular, we find again a continuous decrease of μ_{EO} with increasing Tris concentration for nonporous particles characterizing normal EDL behavior (Figure 4a), while the mobility for porous particles displays pronounced maxima which depend, because of the different intraparticle pore sizes, on mobile phase ionic strength in a particular case (Figure 4b). If we normalize the mobility data for porous particles with respect to the intraparticle EDL overlap (magnitude of the jetting effect) and plot μ_{EO} against r_{pore}/λ_D (Figure 5), we locate the mobility maxima at a similar r_{pore}/λ_D ratio of approximately 10, demonstrating a rather unique dependence of the jetting effect on intraparticle EDL overlap. The slight but systematic shift of this maximum toward lower values of r_{pore}/λ_D at a decreasing pore size (also evidenced by the data for μ_{EP} in Figure 2b) can be explained by the actual differences in R_s/λ_D at a given r_{pore}/λ_D ratio (because of a different λ_D but an almost identical R_s). This reflects the influence of the normal EDL behavior associated with the particles' external surface (cf. Figure 4a) and leads to the relatively stronger decrease in mobility as r_{pore} and λ_D become smaller at constant r_{pore}/λ_D for different particles (Figure 5). Partly in combination with a decreasing ϵ_{intra} (Table 1), that is, the same effect discussed earlier for μ_{EP} (porosity dependence of a particle's dipole coefficient), it is also responsible for the fact that this figure generally reveals higher values of μ_{EO} for particles with larger pore size.

Not unexpectedly, results for μ_{EO} based on the measurement of $\mathbf{u}_{EO}$ in random close packings of the employed spherical particles (fixed beds) did not reveal different electrokinetic behavior than observed by monitoring μ_{EP} for dilute suspensions of the same particles. This is related to the fact that relevant contributions to the overall mobility (jetting effect, dipole coefficient, normal EDL behavior) are similarly influenced by the particles' porosity and intraparticle EDL overlap in either type of experiment. However, one systematic difference is obvious and should be noted. While displaying a very similar behavior, the values for μ_{EO} are generally smaller than those for μ_{EP}. The offset may be largely removed by taking into account the tortuous nature of the pore space between particles in the random close sphere packings, a purely geometrical effect which reduces the macroscopically measured μ_{EO} in

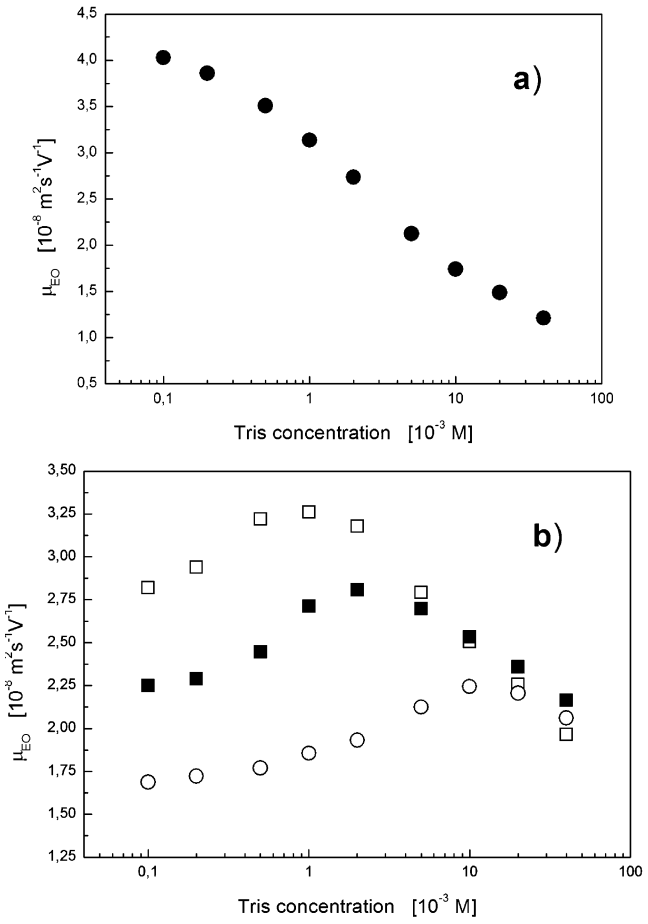

Figure 4. Electroosmotic mobility in fixed beds (packed capillary columns) of the spherical particles depending on the mobile phase Tris concentration: (a) nonporous particles (●); (b) porous particles with a mean intraparticle pore diameter (d_{pore}) of 41 nm (○), 105 nm (■), and 232 nm (□), respectively.

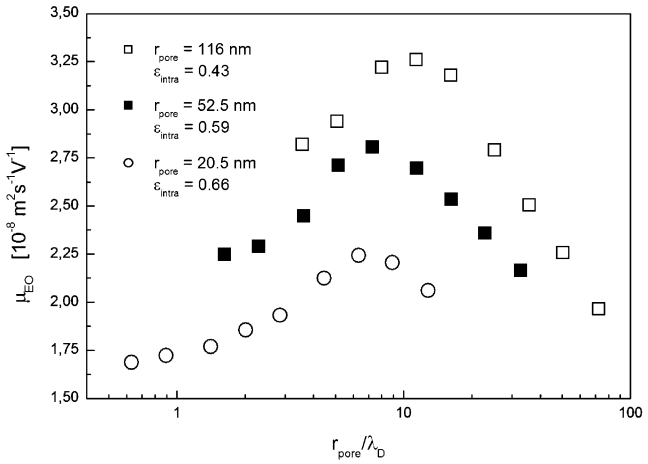

Figure 5. Electroosmotic mobility vs r_{pore}/λ_D for spherical porous particles with a different intraparticle mean pore size and porosity (cf. Table 1).

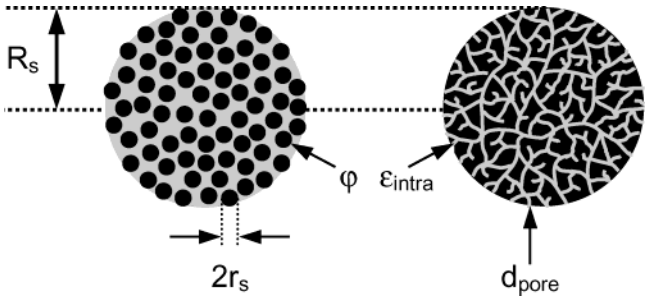

Figure 6. Representation of an aggregated spherical porous particle of radius R_s (with solid volume fraction φ and uniform subparticle diameter d_s) and the particles used in this work (with void fraction ϵ_{intra} and mean pore diameter d_{pore}). In both cases, the pore space morphology and surface chemistry are assumed to be effectively isotropic on the particle scale.

such dense particle systems relative to μ_{EP} for the dilute suspension of an electrophoresis experiment.[96−98]

The consistent dependencies of μ_{EP} and μ_{EO} on both intraparticle porosity and EDL overlap demonstrate a substantially different electrokinetic behavior for porous compared to nonporous particles which has been predicted by Miller et al.[77] However, the final comparison of our data with their theoretical description becomes somehow difficult by a different generation of the pore space morphology within an aggregate or a particle. While porosity and pore size distribution are easily introduced and become adjustable via the diameter and arrangement of much smaller primary particles for a hierarchically structured spherical aggregate,[77,99] porous particles used in this work do not resemble that design. They have been prepared according to the sol−gel process which results in a different microstructure schematically shown in Figure 6. It does not appear straightforward to translate the pore space morphology imposed by the diameter, spatial distribution, and final volume fraction of solid spheres within the aggregate to another particle architecture (e.g., in view of r_s/λ_D vs r_{pore}/λ_D), even though for some special cases the mean size of voids between particles may be estimated based on a touching sphere model.

Consequently, we will compare our results only qualitatively with implications originating from the theoretical work of Miller et al.[77] Based on their analysis, Figure 7 illustrates the dependence of μ_{EP} of a spherical aggregate on EDL overlap (r_s/λ_D) and void volume fraction ($\epsilon_{intra} = 1 - \varphi$) within the aggregate (cf. Figure 6) assuming that the shear plane potential for EOF remains constant and, thus, could be taken as the usual zeta-potential defined for an isolated, discrete solid particle (constant potential assumption concerning EDL overlap in the pores of the aggregate, $\psi_a \equiv \zeta$ in eq 1).[19,77] Figure 7 includes, as a baseline for a better comparison, the mobility of a solid dielectric sphere with $\zeta = 25$ mV and $R_s/\lambda_D \gg 1$. While μ_{EP} decreases with φ at r_s/λ_D below unity due to the normal field component introduced at the outer surface of an aggregate by its conducting interior, this decrease is soon overcompensated with respect to the solid sphere behavior by the jetting effect ($r_s/\lambda_D \geq 7$). As φ is decreasing, the magnitude of this contribution to μ_{EP} can increase significantly in an intermediate r_s/λ_D range (cf. Figure 1)

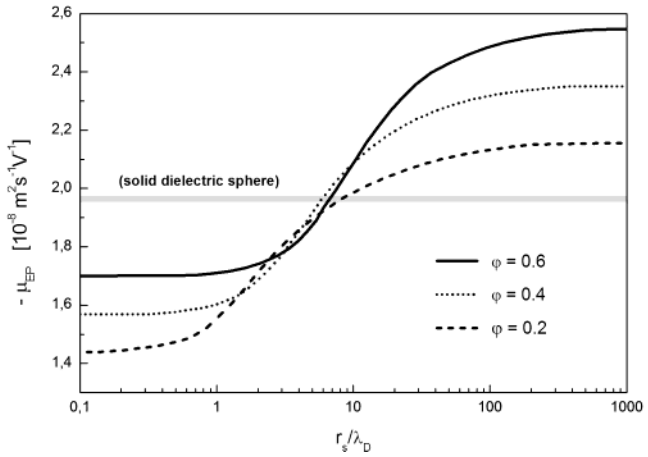

Figure 7. Electrophoretic mobility predicted for a spherical-shaped porous aggregate comprised of solid spheres with $\zeta = 25$ mV and $r_s \ll R_s$ based on the theoretical analysis of Miller et al. (ref 77) (eq 1). The mobile phase is assumed to consist of 80:20 acetonitrile/water (v/v) electrolyte solutions, with $\epsilon_r = 44.53$ and $\eta = 5.03 \times 10^{-4}$ kg/(m·s) at 298 K. F_{EO} at a given r_s/λ_D and φ is obtained from Figure 1.

and, together with the influence of φ on the aggregate's dipole coefficient, porosity differences do not have a strong impact on the net mobility in this regime (Figure 7).

Predictions in Figure 7 indicate that the mobility of a porous aggregate will be significantly less than that of a solid sphere for $r_s/\lambda_D \leq 1$ and significantly greater for $r_s/\lambda_D \geq 20$.[77] They are in qualitative agreement with our experimentally observed dependence of electrokinetic mobility on intraparticle EDL overlap (r_{pore}/λ_D) and porosity (ϵ_{intra}). For example, the data in Figures 2−5 indicate mobility maxima for both μ_{EP} and μ_{EO} of the porous particles in a range $5 < r_{pore}/\lambda_D < 10$. This, in turn, compares favorably with predictions concerning dominating contributions to mobility (with respect to the behavior of a solid sphere) from either a particle's dipole coefficient or the jetting effect, but for obvious reasons (Figure 6) r_s/λ_D is used to characterize EDL interaction in a porous aggregate with known r_s, while it seems straightforward to use r_{pore}/λ_D when the pore size distribution and r_{pore} are available. Apart from the two operative effects (i.e., conducting particle interior and intraparticle EOF) which were shown to cancel each other at specific ionic strengths, another phenomenon relevant to our study is the normal EDL behavior at a particle's external surface. This modifies the reference behavior of the solid, dielectric sphere and asymptotic trends for μ_{EP} of a porous aggregate at low and high r_s/λ_D (Figure 7) accordingly.[78]

5. Conclusions

The experimentally observed dependence on mobile phase ionic strength of electrophoretic and electroosmotic mobilities has revealed substantially different behavior for porous (permeable and conducting) as compared to similar but nonporous (impermeable and nonconducting) spherical particles. While R_s/λ_D remains almost identical for all particles encountered in this work (depending only on ionic strength), r_{pore}/λ_D is further determined by a particular type of porous spheres (Table 1). In addition to the influence of the intraparticle porosity on both μ_{EP} and μ_{EO}, the contribution from the intraparticle EOF has been studied systematically in view of EDL overlap covering the range $0.6 \leq r_{pore}/\lambda_D \leq 72.5$. This, in turn, has allowed us to discriminate between competitive contributions to mobility from a particle's dipole coefficient (intraparticle conductivity) and the jetting effect (intraparticle perme-

(96) Rathore, A. S.; Horváth, Cs. *Anal. Chem.* **1998**, *70*, 3069.
(97) Rathore, A. S.; Wen, E.; Horváth, Cs. *Anal. Chem.* **1999**, *71*, 2633.
(98) Sánchez Muñoz, O. L.; Pérez Hernández, E.; Lämmerhofer, M.; Lindner, W.; Kenndler, E. *Electrophoresis* **2003**, *24*, 390.
(99) Reeder, D. H.; Clausen, A. M.; Annen, M. J.; Carr, P. W.; Flickinger, M. C.; McCormick, A. V. *J. Colloid Interface Sci.* **1996**, *184*, 328.

ability), consistently demonstrated for μ_{EP} (Figures 2 and 3) and μ_{EO} (Figures 4 and 5) with respect to the normal EDL behavior characterizing the nonporous particles. Because most technological and analytical processes involving electrokinetic transport phenomena in porous media like particulate beds use permeable and conducting base material, our results strengthen the importance of the resolved phenomena which can so markedly change electrokinetic behavior compared to solid supports.[77,78] Further, the dependence of macroscopic electrokinetic transport coefficients on the actual pore space morphology, the nature of the surface, and electrolyte properties is of fundamental relevance because it critically guides performance and the design strategies of a particular electrokinetic process with respect to alternative diffusive−convective transport schemes.

Acknowledgment. We are grateful to Dieter Lubda from Merck KGaA (Darmstadt, Germany) for the preparation and characterization of the particle research samples. We further acknowledge financial support by the Landesgraduiertenförderung Sachsen-Anhalt. The authors thank Bernd Ebenau and Dr. Werner Hintz (Institut für Verfahrenstechnik, Otto-von-Guericke-Universität Magdeburg, Germany) for their help with the electrophoretic mobility measurements.

LA0355141